Eur. Phys. J. D **14**, 157–165 (2001)

THE EUROPEAN PHYSICAL JOURNAL D

EDP Sciences

The dynamics of a THz Rydberg wavepacket

A. Wetzels[a], A. Gürtler, H.G. Muller, and L.D. Noordam

FOM-Institute for Atomic and Molecular Physics (AMOLF), Kruislaan 407, 1098 SJ Amsterdam, The Netherlands

Received 23 August 2000 and Received in final form 27 March 2001

Abstract. An optically excited Rydberg wavepacket can be generated by exciting the electron from a low-lying state to a coherent superposition of high-lying states with a short broadband optical pulse. A special kind of Rydberg wavepacket is generated in the case of a interaction of a weak THz half cycle pulse with a stationary Rydberg state, called the THz wavepacket. This THz wavepacket is a coherent superposition of the initial Rydberg state and its neighbouring states. We have investigated the time evolution of THz wavepackets by measuring the impact of two in time delayed half cycle pulses ($\approx$ 200 V cm^{-1}) on the population of a stationary (n = 40) Rydberg state in rubidium. The first half cycle pulse creates the THz wavepacket and the second half cycle pulse probes the dynamics of the THz wavepacket. We support our experimental data by numerically solving the Schrödinger equation and with a semi-classical picture. Whereas an optically excited wavepacket is initially localized, a THz wavepacket is initially delocalized and becomes localized after half a revival time.

PACS. 32.80.Rm Multiphoton ionization and excitation to highly excited states (e.g., Rydberg states) – 03.65.Ge Solutions of wave equations: bound states

1 Introduction

In recent years it has become possible to generate very short freely propagating electrical pulses of half a cycle with a frequency spectrum in the THz regime, often referred to as THz half cycle pulses (HCP) [1–3]. In several experiments the influence of such a HCP on ionization of Rydberg atoms has been investigated [4–7]. If the pulse duration of these HCP is very short compared to the Kepler roundtrip time of a Rydberg electron, the impact of a HCP can be described as a momentum kick

$$\Delta\mathbf{p} = -\int \mathbf{F}(t)\mathrm{d}t \tag{1}$$

to the Rydberg electron where $\mathbf{F}(t)$ is the electric field of the HCP [6,7]. In the limit that the pulse is much shorter than the orbit time the resulting energy transfer is given by

$$\Delta E = \mathbf{p}_0 \cdot \Delta\mathbf{p} + \Delta p^2/2, \tag{2}$$

where $\mathbf{p}_0$ is the initial momentum of the electron. The net energy change will thus depend on the initial momentum of the electron and the direction of the kick.

HCP have been used to probe the dynamics of a Rydberg wavepacket [8–11]. An optically excited Rydberg wavepacket can be generated by exciting the electron from a low-lying atomic state to a coherent superposition of n states with a short optical pulse [12–15]. In order to conserve momentum, optical excitation takes place only near the nucleus; a radially localized Rydberg wavepacket is created [13]. The localized Rydberg wavepacket oscillates in and out about the nucleus with an oscillation period matching the classical period of an electron in a Kepler orbit. The Kepler period is given by the inverse of the energy spacing between the excited n-manifolds ($\tau_{\mathrm{Kepler}} = 2\pi\overline{n}^3$). The long-term evolution of the wavepacket is more complex. The Rydberg states are nearly equally spaced. The deviation from the harmonic spacing causes the wavepacket to spread slowly and in course of time the wavepacket is no longer localized. The spreading is smooth along the orbit until the tail of the wavepacket meets with its head. At this point a new interference pattern begins to form and small wavepackets emerge. This fractional periodicity is called fractional revival. The quadratic regularity of the spacing difference results in a rephasing of the states and the wavepacket becomes localized at $\tau_{\mathrm{revival}} = (\overline{n}/3)\tau_{\mathrm{Kepler}}$. At $\tau_{\mathrm{revival}}/2$ the odd and even states are in phase and the wavepacket is broken up into two discrete wavepacket parts. Only a small fraction of the population is excited from the initial state ($n = \mathrm{i}$) towards higher lying Rydberg states (n), where n is the principal quantum number

$$\Psi = a_\mathrm{i}\psi_\mathrm{i} + \sum_n b_n\psi_n; \qquad \sum_n |b_n|^2 \ll 1. \tag{3}$$

After the excitation the remaining initial state amplitude ($a_\mathrm{i}\psi_\mathrm{i}$) is ignored.

A coherent superposition of Rydberg states can also be generated with a HCP [16–18]. In the case of a strong

[a] e-mail: wetzels@amolf.nl

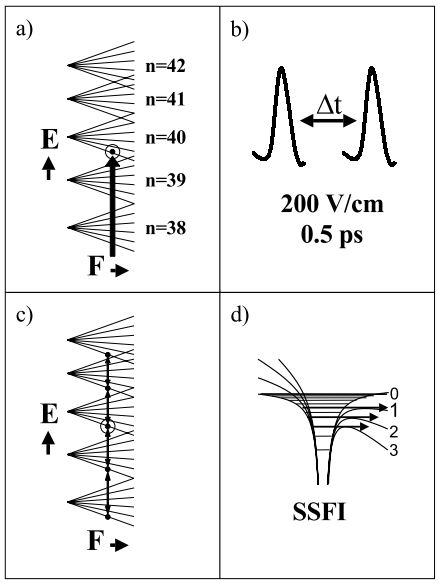

Fig. 1. Schematic illustration of the experiment. (a) Rubidium atoms are laser excited in a static electric field from the ground state to the lower, red, Stark states of the $n = 40$ manifold; the initial Rydberg state. (b) Two HCP kick against the Rydberg electron and change the energy of the electron. The first HCP creates the THz wavepacket and the second probes the dynamics. The delay between the HCP is varied in the experiment. (c) The electron population is redistributed over neighbouring manifolds by the HCP. (d) After the exposure to the THz radiation the final state distribution of the Rydberg atoms was measured by state selective field ionization.

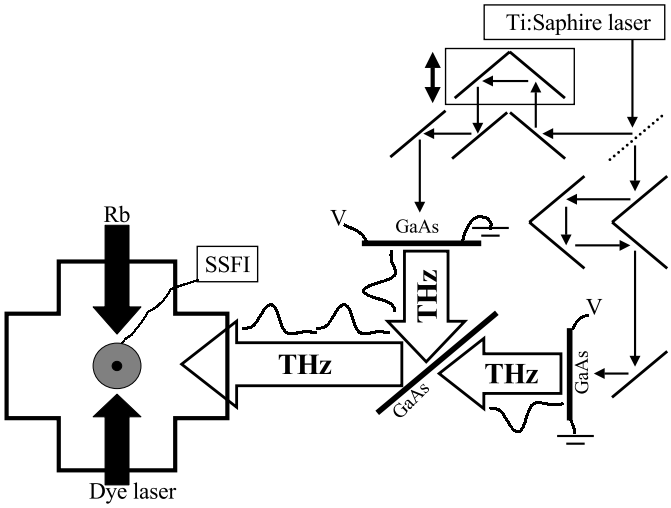

Fig. 2. Schematic representation of the experimental setup (for details see text).

HCP, where the term p^2 in equation (2) dominates, the Rydberg wavepacket is generated by exciting the electron population from a initial low lying state to a superposition of high-lying n states. For small momentum kicks, *i.e.* weak HCP, the second term $\Delta p^2/2$ in equation (2) can be neglected. Starting from the initial Rydberg state n_i the net energy transfer (ΔE) can be both positive ($n > n_\mathrm{i}$) and negative ($n < n_\mathrm{i}$), and the electron population will be spread over neighbouring manifolds, generating a special kind of Rydberg wavepacket, which we will call THz wavepacket. This THz Rydberg wavepacket is a superposition of the initial state and its neighbouring states

$$\Psi = \sum_n a_n \psi_n; \qquad \sum_n |a_n|^2 = 1. \tag{4}$$

Unlike a short optical pulse, the HCP changes the energy of a free electron. Therefore, the electron can increase (or decrease) its energy at any distance from the nucleus. Excitation happens over the full orbit; a delocalized Rydberg wavepacket is created.

We want to investigate the dynamics of this THz wavepackets by comparing the time evolution of the population transferred in the lower-lying neighbouring manifolds ($\Delta E < 0$) with the time evolution of the population in the higher-lying neighbouring manifolds ($\Delta E > 0$) after exposure to a probe HCP. We describe the time evolution of a THz Rydberg wavepacket with a semi-classical picture. A schematic representation of the experiment is given in Figure 1. Rubidium atoms are excited in a static electric field from the ground state to the lower, red, Stark states of manifold $n = 40$ with a nanosecond dye laser. Two HCP are generated by illuminating biased GaAs wafers with a femtosecond Ti:sapphire laser. The first HCP creates a wavepacket and the second HCP is used to probe the dynamics of the wavepacket. The two pulses are delayed in time by a variable delay line in the optical beam. The interaction with the two HCP will change the energy of the electron hence the electron population will redistribute over the neighbouring manifolds. The final state distribution of the Rydberg atoms as a function of the delay between the two HCP is measured by state selective field ionization. The experimental setup is described in Section 2. The final state distribution is also calculated by numerical integration of the Schrödinger equation. The theoretical and experimental data are presented and compared in Section 3. The results are explained with a semi-classical interpretation in Section 4.

2 Experimental setup

The dynamics of a THz wavepacket are investigated by measuring the influence of two HCP on highly excited Rydberg atoms is investigated as a function of the delay between the two HCP. In Figure 2 the experimental setup is shown. Inside a vacuum chamber rubidium was evaporated in a resistively heated oven. Highly excited Rydberg atoms ($n = 40$) were created in a static electric field of 10 $\mathrm{V\,cm^{-1}}$ by two photon excitation ($\lambda = 594.870$ nm) of ground-state rubidium atoms using a Nd:YAG pumped dye laser. The static electric field was strong enough to mix the $41d$ state with the lower, red, Stark states of the $n = 40$ manifold, but too weak to reach the n-mixing regime. Two HCP were created by illuminating biased (≈ 1 kV) GaAs wafers with ≈ 75 fs, 795 nm pulses (≈ 0.1 mJ) from a Ti:sapphire laser. The electric field

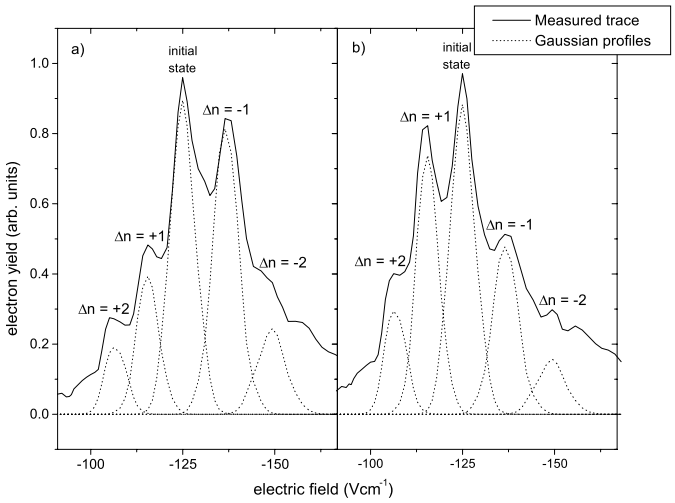

Fig. 3. Measured SSFI traces (straight line) at two different delays between the HCP. In (a) the initial population is transferred to higher-lying, neighbouring Rydberg states, and in (b) to lower-lying, neighbouring Rydberg states. The dotted lines are the Gaussian profiles fitted to the relevant states involved in the wavepacket.

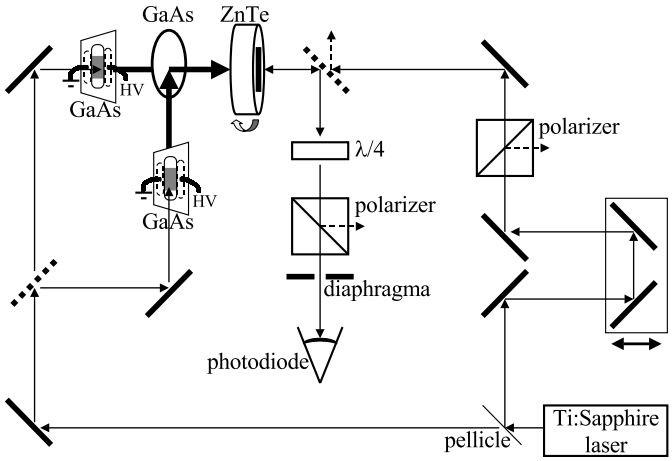

Fig. 4. Illustration of the electro-optical sampling method. The reflected and transmitted beam were detected separately.

of the two HCP in the interaction region, separated by 50 cm from the GaAs wafers, was estimated to be 100–300 V cm^{-1}. The polarization of the HCP was chosen parallel to the static electric field. The polarity of the HCP (either in the $+z$ direction or $-z$ direction) could be altered by changing the polarity of the bias over the wafers. The two pulses were delayed in time by a variable delay line in the optical beam. A third, unbiased, GaAs wafer was used as a beamsplitter to overlap the two HCP in space. The HCP were polarized perpendicular to the plane of incidence (s polarization). The point of overlap of the two HCP in time was determined within 0.5 mm exactly by colinear overlap of the two optical femtosecond beams. Fringes in the optical beams indicated the overlap in time. After the exposure to the THz radiation the final state distribution of the Rydberg atoms was measured by state selective field ionization [19]. In time the electric field was ramped $\approx$ 200 V cm^{-1} in 3 μs, such that the higher Rydberg states would ionize earlier in time than the lower Rydberg states. With state selective field ionization the population in every state could be measured separately. In the SSFI trace the peaks, representing single manifolds, overlapped somewhat, see Figure 3. In this figure the SSFI traces are shown for two different delays between the HCP. In Figure 3a the initial population is transferred to higher-lying, neighbouring Rydberg states, and in Figure 3b the initial population is transferred to lower-lying, neighbouring Rydberg states. The population of each state was determined by fitting a superposition of Gaussian profiles to the measured SSFI trace, see the dotted lines in Figure 3.

The pulse shape of the two HCP after the GaAs beamsplitter was measured by an electro-optical sampling method, (see Fig. 4). The electro-optical sampling method has been described in [20–22]. Briefly, a linearly polarized femtosecond probe pulse, derived from the femtosecond laser propagated collinear with the HCP pulse inside a electro-optic crystal (ZnTe) and probed the change in the index of refraction induced by the electric field of the HCP. In our experiment, the probe pulse was send into the electro-optic crystal from the back surface with respect to the direction of the incoming HCP. The duration of the probe pulse was shorter than the duration of the HCP pulse; therefore the temporal shape of the THz pulse could be measured by changing the relative delay between the THz pulse and the probe pulse while monitoring the phase retardation of the probe beam. The phase retardation was converted into an intensity modulation by passing the probe beam through a polarizer and detecting the transmission with a photodiode. The photodiode signal was integrated and averaged with a boxcar. To get a decent signal-to-noise ratio the data were averaged over ten scans. In Figure 5 the HCP shapes after the GaAs beamsplitter are shown for both the transmitted HCP (Fig. 5a) and the reflected HCP (Fig. 5b). Two peaks appeared, instead of one HCP. The small peak delayed by 11.8 ps with respect to the main peak, was caused by internal reflection of the HCP in the GaAs beamsplitter. The index of refraction at THz frequencies in GaAs is 3.54 and the wafer thickness was 0.5 mm, predicting a delay of 11.9 ps. The polarity of the bias over the GaAs wafers, which generate the HCP were equal for both HCP. So the polarity of the two pulses before the GaAs beamsplitter were equal. But the polarity of the external reflection of the main HCP after the GaAs wafer was opposite to the polarity of the other three pulses. The external reflection of the HCP had flipped polarity on the GaAs beamsplitter as the Fresnel equations predict for s polarized light Gaussian pulse could be nicely fitted to both the main reflected and transmitted HCP. The FWHM of the reflected and transmitted HCP were respectively 0.59 ps and 0.54 ps.

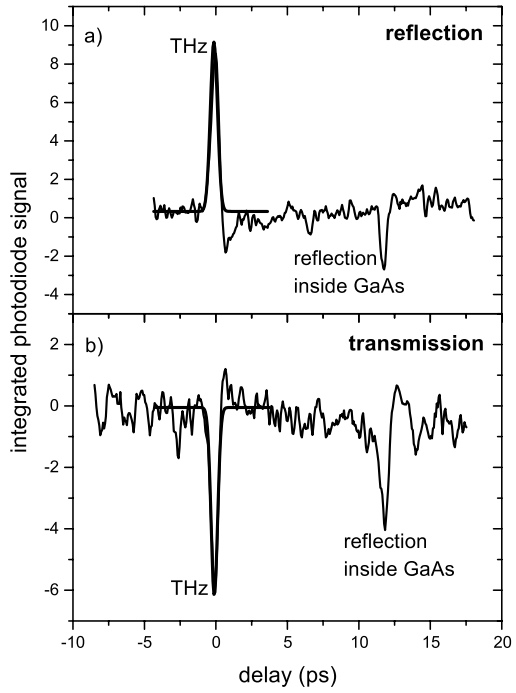

Fig. 5. HCP shape, measured after the GaAs beamsplitter, both (a) the reflected and (b) the transmitted HCP. A Gaussian pulse shape could be nicely fitted to both HCP (thick lines).

3 Results and discussion

3.1 Experimental results

We first discuss the population remaining in the initial state after exposure to THz radiation as a function of the delay between the two HCP. The experiment was done in a static electric field of 10 V cm^{-1}, with as initial state a red Stark state of the $n = 40$ manifold and in zero field, with the $41d$ state as initial state. The results of both experiments are compared. In Figure 6 the fraction of the total population remaining in the initial state as a function of the delay between the two HCP is shown for parallel polarity between the pump and probe HCP. The results for the experiment performed in a static electric field are plotted in Figure 6a and for the experiment performed in zero field in Figure 6b. In the case of opposite polarity between the pump and probe HCP, the fast oscillations have a phase shift of π, these results are not shown. Fast oscillations appear with a period of respectively 10 ps in Figure 6a and 30 ps in Figure 6b. In the experiment performed in a static electric field these fast oscillations equal the Kepler orbit time of the wavepacket; $\tau_{\mathrm{Kepler}} = 9.7$ ps. In the case of the field-free experiment the beat frequency is an average of the transition frequencies from the initial d state to neighbouring p and f states ($\Delta l = \pm 1$); $39f$ (1/22.2 ps), $42p$ (1/39.2 ps), $40f$ (1/31.8 ps), $43p$ (1/16.8 ps). The field-free result agrees with earlier observations [23]. In [23] the experiment was performed with strong HCP, so first order perturbation theory did not hold. In our case, for weak HCP only transitions are allowed when $\Delta l = \pm 1$. For weak HCP the first-order perturbation theory holds. In Figure 6a, the results of the experiment performed in a static electric field, another effect is visible; the fast oscillations decay and revive again over a period of about 123 ps. This period agrees with the revival time of the wavepacket ($\tau_{\mathrm{revival}} = 130$ ps). For the static-electric-field experiment also the population of $\Delta n = \pm 1$ and $\Delta n = \pm 2$ have been measured as a function of the delay between the two HCP. These populations are respectively plotted in Figure 7a for $\Delta n = \pm 1$ and Figure 7b for $\Delta n = \pm 2$, again for parallel polarity between the pump and probe HCP. Fast oscillations, which equal the Kepler orbit time of the electron

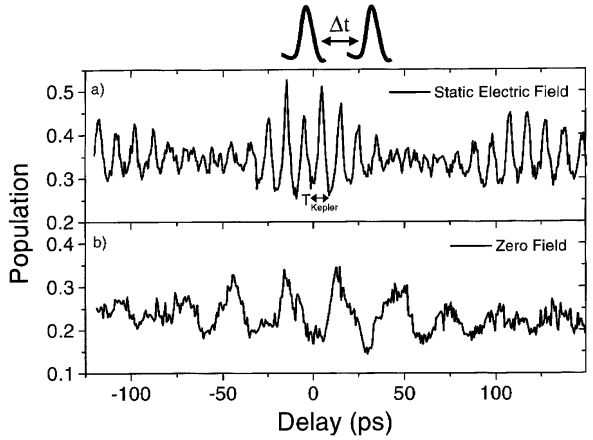

Fig. 6. The population in the initial state after exposure to THz radiation is shown as a function of the delay between the two HCP for (a) in a static electric field and (b) in zero field. The polarity of the two pulses was chosen parallel.

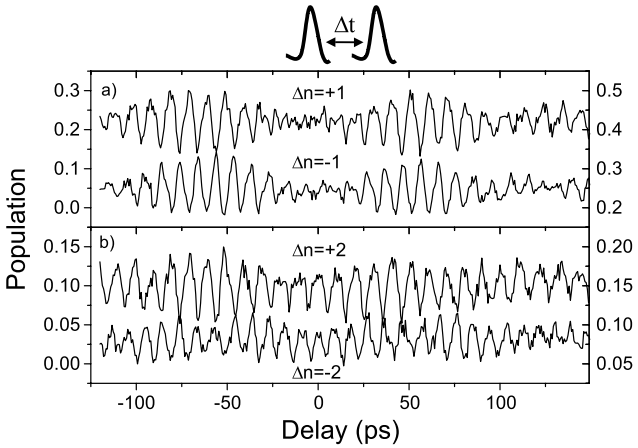

Fig. 7. The population of the neighbouring manifolds after the exposure of the THz radiation is presented as a function of the delay between the two HCP for (a) $\Delta n = \pm 1$ and (b) $\Delta n = \pm 2$. The polarity of the two pulses was chosen parallel. The states are plotted with an offset. Actually the plots overlap. The left axis shows the population for the higher-lying state and the right axis shows the population for the lower-lying state.

are visible. For $\Delta n = \pm 1$ these fast oscillations are out of phase at $\tau_{\text{revival}}/2$. For $\Delta n = \pm 2$ the oscillations are in phase at zero delay, then get out of phase at $\tau_{\text{revival}}/2$ and again in phase at τ_{revival}.

3.2 Theoretical description

The final state distribution for the static-electric-field case was also calculated by numerical integration of the Schrödinger equation. Starting in a stationary, highly excited Rydberg Stark state, two, in time delayed, HCP drive the initial state population to neighbouring states. The population redistribution as a function of the delay can be calculated by numerical integration of the Schrödinger equation:

$$\hbar \frac{\partial}{\partial t} \Psi(t) = -\mathrm{i} H \Psi(t). \tag{5}$$

To simplify the problem we numerically solved equation (5) for the case of a hydrogen atom. In that case the Hamiltonian, H, in a perturbative electric field is:

$$H = -\frac{p^2}{2} - \frac{1}{r} + F(t) z. \tag{6}$$

The perturbation $F(t)$ is given by the electric field of the two HCP. We assume the HCP to be Gaussian in shape and a FWHM of 0.57 ps. Incorporating the observed echo at 11.7 ps (Fig. 5) in the theory might further improve the model but this refinement is beyond the scope of this paper.

The lower, red, Stark states in a manifold couple with the corresponding Stark states in the neighbouring manifolds, *i.e.* the lowest Stark state of a manifold couples only to the lowest Stark states of the neighbouring manifolds. Applying the approximation that initially one Stark state is excited will reduce the amount of states involved in the wavefunction ($\sum c_n \psi_n$) to the amount of manifolds involved. The basis states ψ_n are independent. This requirement produces coupled but separated equations for each c_n, which can be written in matrix form:

$$\hbar \frac{\mathrm{d}}{\mathrm{d}t} \mathbf{c}_n = -\mathrm{i} \hat{H} \mathbf{c}_n. \tag{7}$$

The diagonal elements of the matrix $\hat{H}$ are given by the eigenenergies in zero field and the coupling to the perturbative electric field, the Stark shift Δ_n, multiplied by the perturbative electric field

$$\hat{H}_{n,n} = \frac{1}{2n^2} + \Delta_{n,k} F(t); \qquad \Delta_{n,k} = \frac{3}{2} nk. \tag{8}$$

The off-diagonal elements describe the coupling between the neighbouring states and are given by the semiclassical approximation for transitions between hydrogenic states [24]

$$\hat{H}_{n,n'} = \frac{2}{3\Delta n} J'_{\Delta n}(\Delta n) \sqrt{\Delta_{n,k} \Delta_{n',k'}} F(t), \tag{9}$$

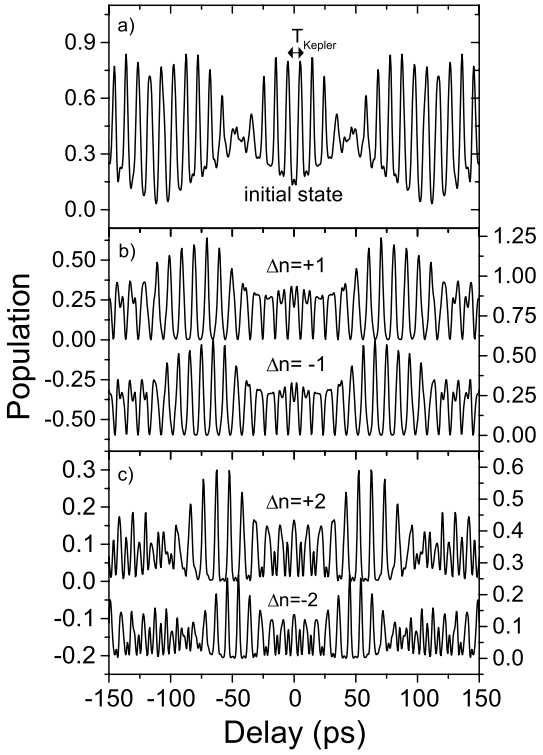

Fig. 8. Calculated populations shown as a function of the delay. In (a) the initial state population is shown, in (b) the population of $\Delta n = \pm 1$ and in (c) the population of $\Delta n = \pm 2$. The polarity was chosen parallel. The higher and lower-lying state in (b) and (c) are plotted with an offset. Actually the plots overlap. The left axis shows the population for the higher-lying state and the right axis shows the population for the lower-lying state.

with $J'_{\Delta n}$ the derivative of the Bessel function of the first kind, order $\Delta n, \Delta n = n - n'$. The ratio of the coupling constant for $\Delta n = 1$ is ≈ 0.2 and for $\Delta n = 2$ this is ≈ 0.07. The ratio continues to fall for increasing Δn.

This first-order differential equation (7) is solved numerically by the fourth-order Runga Kutta integration method. Suppose the initial state in the experiment is a single Rydberg Stark state, then as initial conditions a single amplitude $\mathbf{c}_i$ is put equal to one and all other amplitudes $c_{n \neq i}$ are put to zero.

The theoretical results are shown in Figure 8. The polarity between the two HCP was chosen parallel. The electric field of the two HCP was chosen at 200 V cm^{-1} to get the best quantitative agreement. The population of the initial state, the lowest Stark state of $n = 40$, the population of the lowest Stark states of the $\Delta n = \pm 1$ states and of the $\Delta n = \pm 2$ states are shown respectively in Figures 8a–8c as a function of the delay between the two HCP. In the calculation also the lowest Stark states of the $\Delta n = \pm 3$ states are included to avoid boundary effects. Both in the experiment and in the calculation we found less than 4% population in the $\Delta n = \pm 3$ states. In agreement with our experimental data we observe fast

oscillations (9.8 ps) equal to the Kepler orbit period. The fast oscillations in the initial state decay and revive again over the revival time of the wavepacket ($\tau_{\rm revival} \approx 125$ ps). At zero delay the oscillations in $\Delta n = \pm 1$ are in phase, near $\tau_{\rm revival}/2$ these oscillations are out of phase and get in phase again near one revival time. These results are in agreement with the experimental observations. The oscillations in $\Delta n = \pm 2$ are in phase at zero delay and at integer multiples of $\tau_{\rm revival}/2$, in between the oscillations are out of phase. In the final population of $\Delta n = \pm 2$ fast oscillations appear with a periodicity of half the Kepler period ($\tau_{\rm Kepler}/2$), indicating direct, one photon, transition from the initial state to the $\Delta n = \pm 2$ states, besides the two transition steps of $\Delta n = \pm 1$. These direct $\Delta n = \pm 2$ transitions are also the reason that the oscillations in the $\Delta n = \pm 2$ states are in phase at half the revival time of the wavepacket. This does not agree with the experimental results where we observe only $\Delta n = \pm 1$ transitions. In the experimental results no indication is found for direct, one photon, transition to the $\Delta n = \pm 2$ states. The signal to noise ratio of the experiment is not sufficient to exclude any $\Delta n = 2$ one-photon transitions, but the theory clearly overestimates the contribution of this process.

In the calculations two equal HCP were used, while in the experiment the HCP might not be equal, since they were generated from different GaAs wafers. Taking this into account in the calculation, different pulse duration and electric field strength, did not improve the agreement. Small differences between the two HCP hardly affected the theoretical results, while for large differences the out and in phase time in $\Delta n = \pm 2$ became irregular. This tells us, that our two HCP are almost equal in shape. It does not give us an explanation for the difference between theory and experiment. The Fourier transform of the Gaussian HCP shows that the frequencies of both the $\Delta n = \pm 1$ transitions and $\Delta n = \pm 2$ transitions are present, indicating that both transitions should be allowed. Maybe the coupling constant for $\Delta n = \pm 2$ transitions is overestimated in the theoretical calculations. We compared the approximated matrix elements of equation (9) with exactly calculated matrix elements. First the eigenstates of rubidium in a static electric field of 10 V cm^{-1} for $m = 0$ where determined. Next the coupling constants were calculated between every eigenstate. The ratios of the exactly calculated coupling constants to the coupling constant of $\Delta n = 0$ are the same as our simplified equation (9) predicts, namely ≈ 0.2 for $\Delta n = \pm 1$ transitions and ≈ 0.07 for $\Delta n = \pm 2$ transitions. This exact calculation also showed that lower, red, Stark states couple with the corresponding Stark states in the neighbouring manifolds, as already mentioned in the beginning of this section. In the experiment the bandwidth of the dye laser was not small enough to excite one Stark state, probably several Stark states were excited. Taking this into account in our theoretical calculation by defining the final state populations as a summation over several Stark states, did not improve the agreement. In conclusion our experimental and theoretical results agree, except for the direct $\Delta n = \pm 2$ transitions.

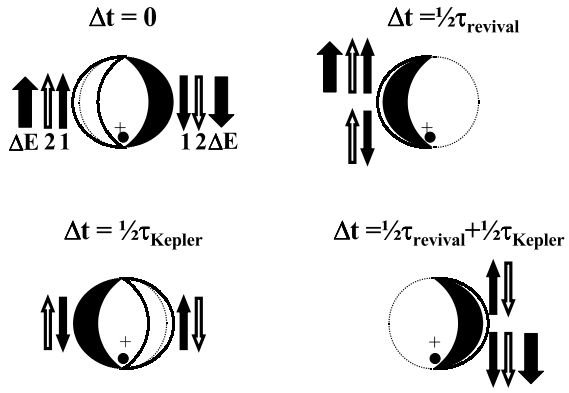

Fig. 9. Semi-classical picture describing the experiment. The initial state, a standing wave, is described by two counter propagating waves, illustrated by the white and black part. The situation is shown at four different delay times, respectively at delay = 0 s, delay = $\tau_{\rm Kepler}/2$, delay = $\tau_{\rm revival}/2$ and delay = $\tau_{\rm revival}/2 + \tau_{\rm Kepler}/2$. The influence of the first half cycle on each wave is shown by the small black arrow, the influence of the second HCP by the white arrow. The big black arrow shows the net energy change.

The importance of these transitions as indicated by the theory is not confirmed in the experiment.

4 Semi-classical interpretation

4.1 Semi-classical picture

In this section we present an intuitive semi-classical picture to explain the measured and calculated results, illustrated in Figure 9. Let us describe the initial Rydberg state, a standing wave, as two counter propagating waves. In Figure 9 these two propagating waves, moving along the orbital, are illustrated by the white and black part. The black fraction represents the wave moving towards the nucleus and the white represents the outgoing wave. Suppose the direction of the momentum kick of the first HCP increases the energy of the white wave. Then the first HCP will decrease the energy of the other, black wave, because for this wave the momentum is opposite in sign. The effect of the first HCP is shown by the small black arrows. If the second HCP interacts with the atom at the same time as the first HCP (delay = 0 s) and has the same polarity, then the second HCP will have the same effect on the electron, illustrated by the white arrows. So it will also increase the energy of the white wave and decrease the energy of the black wave. The net energy change, shown by the big black arrows will be equal in magnitude for both waves, but opposite in sign. This will result in electron transitions from the initial manifold to both higher and lower n-manifolds. Let us now consider what happens if the second HCP arrives half a Kepler roundtrip time later than the first HCP (delay = $\tau_{\rm Kepler}/2$). The initial momentum of the electron will have changed sign in the

meantime and the effect of the second HCP will be opposite to the effect of the first HCP. The kick of the second HCP cancels the energy change caused by the kick of the first HCP. So the energy change of both waves will be zero: the electrons stay in their initial state. When the delay is equal to one Kepler roundtrip time the situation will be almost equal again to zero delay. The electrons will move to both higher and lower states. In summary, if the delay between the HCP is small we will notice that respectively the electrons move to both higher and lower states and half a Kepler roundtrip time later they will stay in the initial state. The oscillations of the final population of the higher and lower states. This is what we also observe in our data (Figs. 6a and 7).

If the delay between the two pulses equals half the revival time of a wavepacket, the two initially counter-propagating waves are now co-propagating, *i.e.* the waves are at the same side of the orbit and propagate in the same direction. So their momentum will be equal. As a result the second HCP will have the same effect on both waves. Suppose that the second HCP increases the energy of the waves, then the net energy after exposure to both HCP will be increased for the white wave and for the black wave the energy change caused by the first HCP will be cancelled by the second HCP. A fraction of the population will move to higher manifolds and the rest will stay in the initial state. If the second half cycle pulse arrives half a revival time plus half a Kepler roundtrip time later than the first HCP (delay $= \tau_{\mathrm{revival}}/2 + \tau_{\mathrm{Kepler}}/2$) the second HCP will decrease the energy of both waves, because the initial momentum of the electrons has changed sign again. The net energy gain after exposure to both HCP will be zero for the white wave while decreased for the black wave. Again a part of the population stays in the initial state and the rest will move to lower manifolds. In summary, near $\tau_{\mathrm{revival}}/2$ the population in the initial state remains constant and a part of the population will move alternating to higher and lower manifolds. The oscillations in the final population of the higher and lower n-states are out of phase. This behavior we see in our data (Figs. 6a and 7).

The same semi-classical interpretation holds for antiparallel polarity of the HCP as well. The only difference is that for the same momentum of the electron the effect of the second HCP will be opposite to the effect of the first HCP. This will lead to a phase shift of π in the fast oscillations.

4.2 Calculation

We determined the expectation value of the z-coordinate (direction parallel to the electric field) of the wavepacket in time to support our semi-classical interpretation. When the wavepacket parts are counter propagating, *i.e.* the wavepacket is delocalized, we expect to see an averaged, constant z-coordinate. When the wavepacket parts are co-propagating, *i.e.* the wavepacket is localized, the z-coordinate will oscillate between its extremes. The parabolic eigenfunctions ψ are, as determined by Bethe and Salpeter [25]

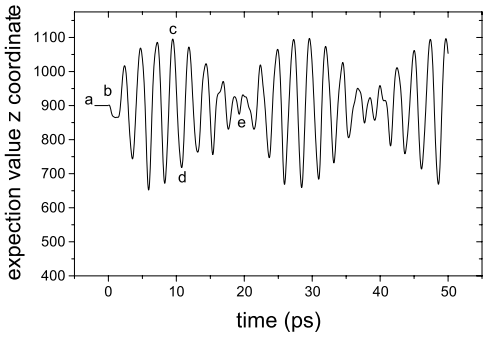

Fig. 10. The expectation value of the z-coordinate (direction parallel to the electric field) is plotted as a function of time. The maximum of the HCP is at zero ps. As can be seen the wavepacket is initially delocalized, no oscillations, and after $\tau_{\mathrm{revival}}/2$ localized.

$$\psi_{n_1,n_2,m} = \frac{\mathrm{e}^{\pm \mathrm{i}m\varphi}}{\sqrt{\pi n}} \frac{{n_1!}^{\frac{1}{2}} {n_2!}^{\frac{1}{2}} \varepsilon^{m+\frac{3}{2}}}{{(n_1+m)!}^{\frac{3}{2}} {(n_2+m)!}^{\frac{3}{2}}} \mathrm{e}^{-\frac{1}{2}\varepsilon(\xi+\eta)} (\xi\eta)^{\frac{1}{2}m} \times L^m_{n_1+m}(\varepsilon\xi) L^m_{n_2+m}(\varepsilon\eta) \quad (10)$$

$$n_1 = \frac{n+k-1-|m|}{2}, n_2 = \frac{n-k-1-|m|}{2} \cdot \quad (11)$$

The amplitudes of the eigenstates after the first HCP kick, the kick which generates the wavepacket, can be determined in time as mentioned in Section 3.2 by numerical integration of the Schrödinger equation, with one difference: the perturbation $F(t)$ is given by the electric field of one HCP.

Because of computation problems at high n-manifolds, the calculation is done around $n = 25$. The electric field $F(t)$ and the pulse duration of the HCP have to be scaled. To stay in the impulsive regime the ratio of the pulse duration of the HCP to the Kepler round trip time has to be constant. The electric field of the HCP is scaled to ensure an equivalent amount of population transferred to Δn. It turns out that the electric field of the HCP has to be proportional to $\overline{n}^{-4}$

$$\tau_{\mathrm{HCP}} \propto \tau_{\mathrm{Kepler}} \propto \overline{n}^3 \quad (12)$$

$$F_{\mathrm{HCP}} \propto F_{\mathrm{ionization}} \propto \overline{n}^{-4}. \quad (13)$$

So the electric field F and the pulse duration used in the calculation are respectively 1311 $\mathrm{V\,cm^{-1}}$ instead of 200 $\mathrm{V\,cm^{-1}}$ and 0.138 ps instead of 0.57 ps. The eigenstates involved are the lowest Stark states of the manifolds $n = 23{-}28$ instead of manifolds $n = 37{-}43$.

The expectation value of the z-coordinate is plotted in Figure 10 as the wavepacket evolves in time. The maximum of the HCP is at 0 ps. At negative times the expectation value of the z-coordinate of the initial, stationary state is constant in time and of the order $(3/2)n^2 a_0$, which we would expect for a standing wave. After exposure to THz radiation, at positive times a wavepacket is formed. The initially standing wave can be described as

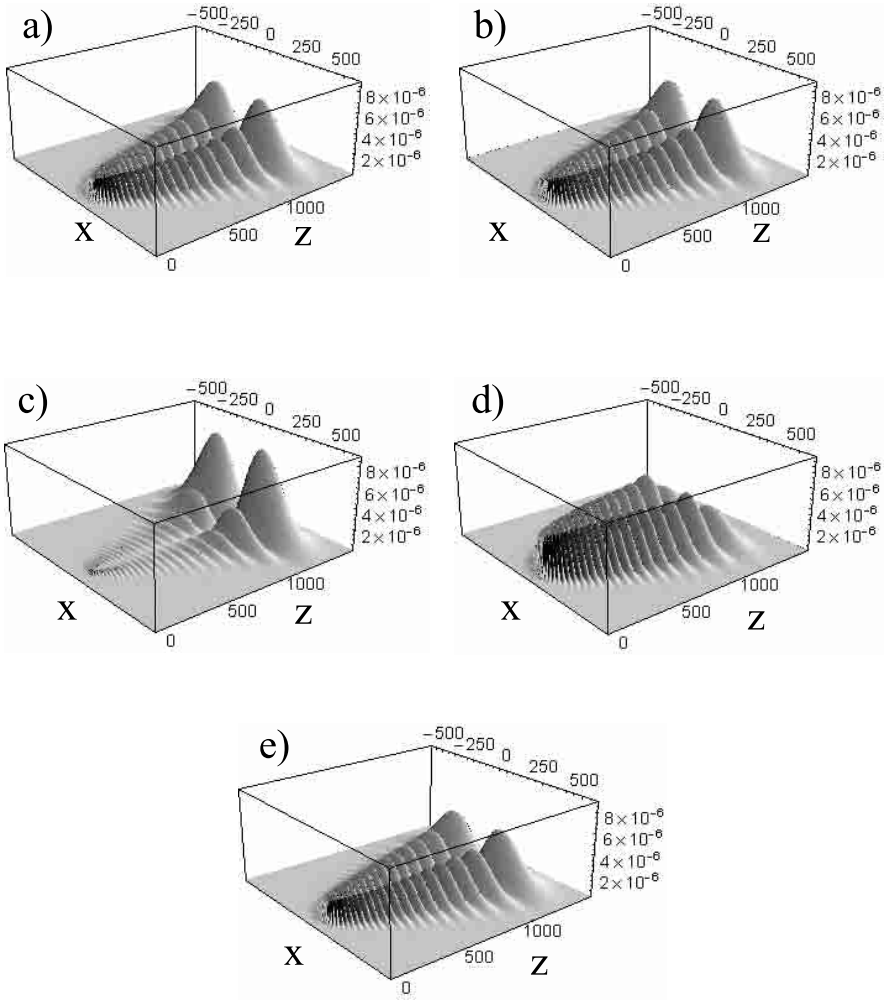

Fig. 11. The wavepacket is plotted at specific timepoints, denoted in Figure 9 with the letters a–e, to illustrate the dynamics of the wavepacket. In figure a the standing wave is plotted. The population is distributed over the whole orbital. In (b), during the interaction of the HCP with the Rydberg atom, the population is still distributed over the whole orbit (delocalized), which one can describe as two counter-propagating waves. In (c) and (d) the two initially counter-propagating waves are co-propagating. The population is localized on the orbit. In (c) the two co-propagating waves are at the outer turning point. In (d) the two co-propagating waves are at the inner turning point. In (e) the two former co-propagating waves are counter-propagating again and the population is distributed over the whole orbit.

two counter-propagating waves. The wavepacket will be delocalized over the orbit and therefore the expectation value of the z is still constant in time. As we approach $\tau_{\text{revival}}/2$ the two initially counter-propagating wavepacket parts are now co-propagating, the wavepacket is localized on the orbit. The z-coordinate starts to oscillate, with an oscillation period equal to the Kepler orbit time ($\tau_{\text{Kepler}} = 2.37$ ps for $n = 25$). The oscillation amplitude increases until it reaches its maximum at $\tau_{\text{revival}}/2$, where the population is fully localized. The localized wavepacket moves in and out the core region, causing large oscillations in the z-coordinate. Hereafter the oscillations decay as the wavepacket gets slowly delocalized. The expectation value of the z-coordinate is constant again at one revival time ($\tau_{\text{revival}} = 19.5$ ps). The wavepacket is fully delocalized again. In Figure 11 we plotted the wavepacket at specific times, denoted in Figure 10 with the letters a–e, to make the dynamics of the wavepacket visible. The population $\left(\Psi^2\right)$ is plotted in the xz-plane (z-direction parallel to the electric field) after integration over the y coordinate. The wavepacket is symmetric in the xy-plane ($m = 0$).

5 Summary

We investigated the dynamics of a THz wavepacket both experimentally and theoretically. Such a THz Rydberg wavepacket differs from conventional Rydberg wavepackets. In a THz wavepacket the initial state, out of which the coherent superposition of wavepacket states is populated, is part of the wavepacket. In the experiment a delayed, THz probe pulse, monitors the dynamics of the wavepacket. We found oscillations in the final population as a function of the delay between the two HCP. In the presence of a small static electric field these oscillations match the Kepler orbit frequency, while in absence of a static electric field the oscillation frequency is given by the dipole allowed transitions from the initial state. The calculations are performed by numerical integration on the Schrödinger equation. These calculations confirm our observations on the population redistribution, in particular when the population oscillations of the different Rydberg states are in and out of phase. Oscillations with a frequency matching a direct $\Delta n = \pm 2$ transition are predicted by theory but not found in the

experiment. We have no explanation for this discrepancy. Further insight in the dynamics is obtained by a semi-classical picture, using that a standing wave can be described by two counter-propagating waves. We supported our semi-classical picture by calculating the expectation value of the z-coordinate as the wavepacket evolves in time and by plotting the wavepacket at specific time points. The short-term evolution, the Kepler orbit motion, and the long-term evolution, the decay and revival of the wavepacket, of a THz wavepacket are comparable with the short-term and long-term evolution with a optical wavepacket. The large difference is that an optically excited wavepacket is initially localized, whereas a THz wavepacket is initially delocalized and becomes localized after $\tau_{\mathrm{revival}}/2$.

We would like to thank F. Robicheaux for fruitful discussions. It is a pleasure to acknowledge the skillful assistance of R.B. Vrijen in early stages of the experiment. We would also like to thank Florentina Roşca-Prună, Céline Nicole, Anton Buyserd and Mark Vrakking for providing the femtosecond laser beam. We acknowledge EU-Network Cocomo, HPRNT-CT-1999-00129. The work described in this paper is part of the research program of the FOM (Foundation for Fundamental Research on Matter) and was made possible by the financial support from NWO (Netherlands Organization for the Advancement of Research).

References

1. B.B. Hu, J.T. Darrow, X.-C. Zhang, D.H. Auston, Appl. Phys. Lett. **56**, 886 (1990).
2. B.B. Hu, X.-C. Zhang, D.H. Auston, Phys. Rev. Lett. **67**, 2709 (1991).
3. D. You, R.R. Jones, P.H. Bucksbaum, Opt. Lett. **18**, 290 (1993).
4. R.R. Jones, D. You, P.H. Bucksbaum, Phys. Rev. Lett. **70**, 1236 (1993).
5. R.R. Jones, N.E. Tielking, D. You, P.H. Bucksbaum, Phys. Rev. A **51**, R2687 (1995).
6. R.B. Vrijen, G.M. Lankhuijzen, L.D. Noordam, Phys. Rev. Lett. **79**, 617 (1997).
7. F. Robicheaux, Phys. Rev. A **56**, R3358.
8. C. Raman, C.W.S. Conover, C.I. Sukenik, P.H. Bucksbaum, Phys. Rev. Lett. **76**, 2436 (1996).
9. M.T. Frey, F.B. Dunning, C.O. Reinhold, J. Burgdörfer, Phys. Rev. A **55**, R865 (1997).
10. C. Raman, T.C. Weinacht, P.H. Bucksbaum, Phys. Rev. A **55**, R3995 (1997).
11. M.B. Campbell, T.J. Bensky, R.R. Jones, Phys. Rev. A **59**, R4117 (1999).
12. J. Parker, C.R. Stroud Jr, Phys. Rev. Lett. **56**, 716 (1986).
13. A. ten Wolde, L.D. Noordam, H.B. van Linden van den Heuvell, Phys. Rev. Lett. **61**, 2099 (1988).
14. J.A. Yeazell, M. Mallalieu, C.R. Stroud Jr, Phys. Rev. Lett. **64**, 2007 (1990).
15. Z.D. Gaeta, C.R. Stroud Jr, Phys. Rev. A **42**, 6308 (1990).
16. C.O. Reinhold, J. Burgdörfer, M.T. Frey, F.B. Dunning, Phys. Rev. A **54**, R33 (1996).
17. R.R. Jones, Phys. Rev. Lett. **76**, 3927 (1996).
18. J. Bromage, C.R. Stroud Jr, Phys. Rev. Lett. **83**, 4963 (1999).
19. T.F. Gallagher, *Rydberg Atoms*, 1st edn. (University Press, Cambridge, 1994).
20. Q. Wu, X.-C. Zhang, Appl. Phys. Lett. **67**, 3523 (1995).
21. A. Nahata, D.H. Auston, T.F. Heinz, C.Wu, Appl. Phys. Lett. **68**, 150 (1996).
22. P.U. Jepsen, C. Winnewisser, M. Schall, V. Schyja, S.R. Keiding, H. Helm, Phys. Rev. E **53**, R3502 (1996).
23. N.E. Tielking, R.R. Jones, Phys. Rev. A **52**, 1371 (1995).
24. J. Picart, A.R. Edmonds, N. Tran Minh, J. Phys. B **11**, L651 (1978).
25. H.A. Bethe, E.E. Salpeter, *Quantum Mechanics of One- and Two-Electron Atoms*, paperback edn. (Plenum, New York, 1977).